INTERNATIONAL JOURNAL OF
Applied Glass
SCIENCE

Melt Homogenization and Self-Organization in Chalcogenides-Part II

Siddhesh Bhosle, Kapila Gunasekera,* and Punit Boolchand*†

School of Electronics and Computing Systems, College of Engineering and Applied Science, University of Cincinnati, Cincinnati, Ohio 45221-0030

Matthieu Micoulaut

Laboratoire de Physique Theorique de la Matiere Condensee, Universite Pierre et Marie Curie Boite 121, 4 Place Jussieu, 75252, Paris Cedex 05, France

The compositional variation of the non-reversing enthalpy at T_g, $\Delta H_{nr}(x)$, in Ge_xSe_{100-x} glasses decreases abruptly by an order of magnitude as x increases to $x_c(1) = 19.5(5)\%$, the rigidity transition, and then remains minuscule till x increases to $x_c(2) = 26.0(5)\%$, when the term abruptly increases by an order of magnitude as glasses become stressed-rigid. The rigid but unstressed networks formed in between these two transitions represent the Intermediate Phase (IP). The square-well like variation of $\Delta H_{nr}(x)$, also known as the reversibility window develops sloping walls, then a triangular shape and eventually disappears as glasses of increasing heterogeneity are studied. The ΔH_{nr} term ages over weeks outside the IP but not inside the IP. Raman line shapes of *as-quenched melts* are quite similar to those of T_g-*cycled glasses* for compositions in the IP, but not outside the IP– an optical analog of the thermal reversibility window. Variations of Molar volumes, display a global minimum in the IP and a pronounced increase outside that phase. Physical behavior of dry and homogeneous chalcogenide glasses that leads to sharp *elastic* and *chemical* phase transitions remains to be understood theoretically. The physics of network may be even more interesting than hitherto recognized.

Introduction

Bulk glass formation occurs in insulating, semiconducting, metallic and H-bonded materials systems, but in selected range of chemical compositions. What is so special about these select melt compositions that can be cooled slowly to bypass crystallization and yield large (gram sized) bulk glasses? Important clues to understanding this unusual behavior evolved from Rigidity theory and experiment,[1–13] which have shown that bulk glass formation usually occurs in ranges when networks become isostatic[1] at an optimal connectivity. The theory starts from fundamental interactions including bond-stretching and bond-bending forces between atoms, and identifies metastability of

covalent glassy networks in terms of *non-local internal network stress*, and not intensive free energies. Thorpe[2,12] independently identified a new class of cyclical or floppy modes in simulations of realistically compacted yet fully disordered 3D mean-field models. By establishing the count of floppy modes as a function of the number of central and non-central valence bond forces – Phillips[1] and Thorpe[2,12] discovered the *Stiffness Transition*- the connectivity related flexible to stressed-rigid elastic phase transition, which has become the focus of modern theory of network glasses. To test these elegant ideas much experimental work[3–5,8,9,11,13] has continued in the field since the mid-1980s. And as data on several families of covalent and ionically modified covalent systems evolved, it emerged starting in the late 1990s that there are actually two distinct elastic phase transitions[4,5,11] and not just one as predicted. These two transitions now widely recognized,[3–13] are the *rigidity* transition followed by a *stress* transition observed at slightly higher network connectivity. In *random* networks these two transitions coincide, i.e., rigidity and stress both nucleate once the network connectivity exceeds the stiffness transition value of $\bar{r} = 2.40$ for 3D systems. Here $\bar{r}$ represents the mean coordination number of a network. In real systems, networks apparently reconnect[6,8] to minimize stress when $\bar{r}$ is near 2.40, with the opening of an intervening region between the onset of *rigidity* and that of *stress transitions known as the Intermediate phase.* The phase represents a rigid but stress-free state of disordered matter.[3,8,12] Experiments also show that the Intermediate Phase (IP) glass compositions possess unexpected physical properties,[4,5,8,13] they possess almost thermally reversing glass transitions[14,15] that barely age, display characteristic elastic power-laws, and form space filling networks. Recently it was shown[16] that the thermally reversing character of the glass transition is a consequence of the isostatic nature of such networks.

We have recently addressed[17] some of the challenges in synthesizing homogeneous non-stoichiometric $Ge_x Se_{100-x}$ glasses (see Part I). Herein we report[17,18] on the optical, thermal, and mechanical properties of these specially synthesized glasses, which provide striking evidence of three *abrupt* transitions, two elastic and one chemical in nature; a rigidity transition near $x_c(1) = 19.5(3)\%$, stress transition near $x_c(2) = 26.0(3)\%$, and a chemical transition near $x_c(3) = 31.5(3)\%$. The finding of sharp elastic phase transitions, we hope will stimulate discussions amongst theorists and experimentalists alike, and assist in unraveling the fundamental nature of these *critical points* including the elusive nature of glass transition.[19]

Dispersive Raman Scattering

All Raman scattering measurements on glasses made use of a dispersive system (Model T 64,000; Horiba, Jobin Yvon Inc). A 5 mW of 647 nm radiation from a Kr-ion laser with a 50 µm spot size was brought to a line focus on a glass sample wetting the inside surface of evacuated quartz tubes. Laser-power density was ~10 W/cm^2, and kept low to suppress photo-structural effects[5,11] in these soft materials. The back scattered radiation was analyzed in the triple subtractive mode using a CCD Detector. An accumulation typically lasted 2 min. The advantages of using red (647 nm) instead of NIR radiation (1064 nm) to obtain complete and reliable DOVS in glasses was mentioned earlier in Part I. Figure 1 displays spectra at a few glass compositions in the $Ge_x Se_{100-x}$ binary. The observed lineshapes were analyzed as a superposition of Gaussians using Peak Fit software (Fig. 2). Raman lineshapes of as-quenched melts were compared to T_g-cycled glasses in Fig. 3, and show these to be almost identical in the narrow compositional window, $20\% < x < 26\%$, but not outside that select window.

Modulated Differential Scanning Calorimetry (mDSC)

A model 2920 mDSC from TA Instruments Inc. was used to investigate the nature of glass transitions. The instrument can be operated in either the DSC or the mDSC mode. The m-DSC mode offers the advantage of providing the total heat flow (as in DSC) and also the reversing- and the non-reversing heat flow components[20,21] (Fig. 4) that make up the total heat flow. In all measurements we used a 3°C/min scan rate, 1°C T- modulation amplitude, and 100s modulation period to examine glass transitions.

The component of the total heat flow that tracks the programmed sinusoidal T- oscillations is the *reversing heat flow*. It captures quasi-equilibrium thermodynamic properties of the metastable glass state, specifically its heat-capacity jump (ΔC_p), and T_g established from
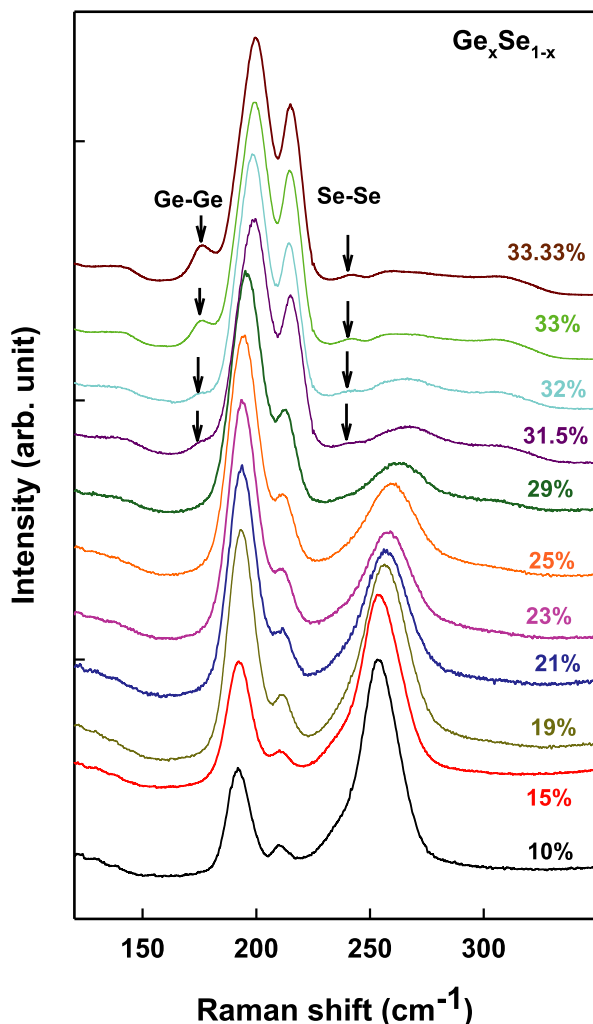
Fig. 1.   *Raman scattering of homogenized Ge$_x$Se$_{100-x}$ glasses show growth in scattering strength of modes of Corner-Sharing (200/cm) and Edge-Sharing (217/cm) tetrahedra at the expense of the Se$_n$ chain mode (250/cm) as x increases in the 10% < x < 33.33% range. At x > 31.5%, a pair of new modes appears near 247 and 180/cm, and their scattering strength increases with x. These modes are identified with Se-Se and Ge-Ge stretch vibrations in Se-rich and Ge-rich nanophases, respectively.*

Fig. 2.   *Raman line shape of a bulk glass at x = 20% deconvoluted in terms of Gaussians using Peak Fit software. The FWHM, centroid and scattering strength of the CS mode (green), the ES mode (yellow) and the Se$_n$ chain mode (brown) were obtained.*

wide range in x. A parallel result of $\Delta C_p(x)$ was noted earlier on the Ge$_x$As$_x$Se$_{100-2x}$ ternary[22] (Fig. 5b).

We have fit the $T_g(x)$ variation in glasses to a polynomial, resulting in Eq. (1) below.

$$T_g(x) = 39.781 + 8.702x - 0.271x^2 + 0.011x^3 \quad (1)$$

The smooth line in the plot of Fig. 5a is a plot of eq. (1), and it reproduces the observed $T_g(x)$ variation to an accuracy of 2°C. The monotonic increase of $T_g(x)$ also provides a check on glass composition x, and can be used to estimate the error in x, which we place near 0.1%. The slope dT_g/dx reaches a maximum near $x = 31.5\%$ (Fig. 5a). We also observe a sharp cusp in the non-reversing enthalpy $\Delta H_{nr}(x)$ near $x = 31.5\%$, and a reduction at higher x, which is signature of a loss of network connectivity due to nanoscale phase separation[23] of the backbone.

At select compositions DSC experiments were performed at a scan rate of 10°C/min (Fig. 6), which have permitted comparison with earlier reports. The results of Sreeram et al.[24] are quite close to the present ones at $x = 10\%$ and 23%, but less so at other compositions. The data of Guin et al.[25] show a broad trend similar to the present results except their $T_g(x)$ values are consistently 10–15°C lower than the present results. We have also measured T_g of present homogenized glasses that were wet, and find these to be about 10°C lower than the dry ones (see Table I in Part I). These observations suggest that the glass samples reported in Refs. 24–26 are probably not as dry as the present ones.

the inflexion point. Scan rate-related kinetic shifts are eliminated by averaging T_g obtained in a heating cycle followed by a cooling one. The typical error in T_g is 2° C. Compositional trends in $T_g(x)$ and $\Delta C_p(x)$ appear in Figs. 5a and b, respectively, and show that while T_g increases monotonically with x, $\Delta C_p(x)$ terms remain independent of x near a value of 0.035 cal/g across a
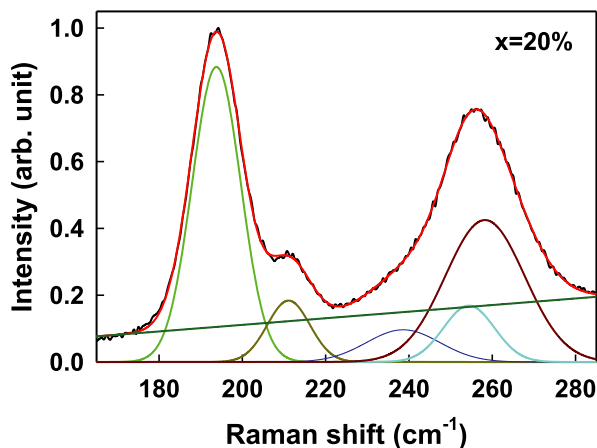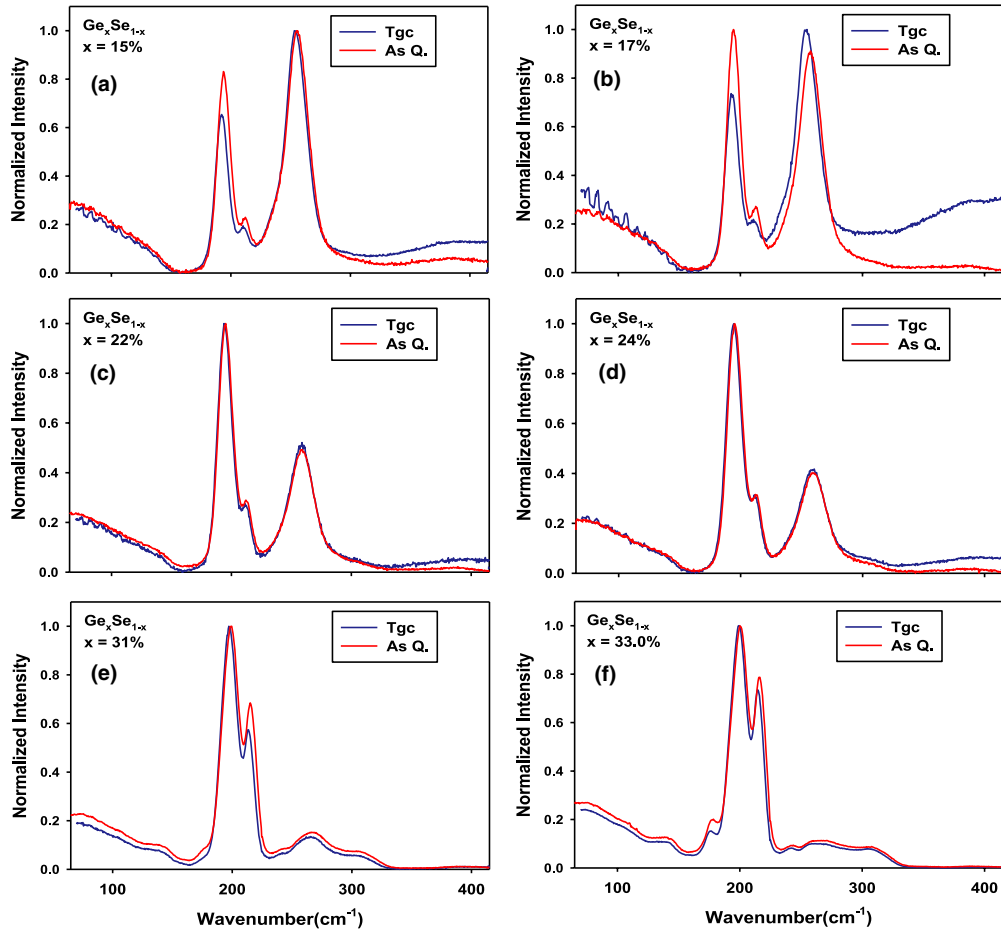
Fig. 3.   Raman scattering of melt-quenched glasses taken before and after T_g cycling. At (c) x = 22% and (d) 24% (in the IP), spectra of the as-quenched melts are almost identical to those of T_g-cycled glasses, but such is not the case for compositions, (a) x = 15%, (b) 17%, (e) 31% and (f) 33.0% that are outside the IP.

One of the *first* indications that glass compositions in the range, 20% < x < 26%, behave differently from others emerged from the enthalpy $\Delta H_{nr}(x)$. In an mDSC measurement by subtracting the integrated area under the peak observed upon cooling (exotherm) from the peak observed upon heating (endotherm), one obtains (Fig. 4) the modulation frequency corrected $\Delta H_{nr}(x)$ term.[20,21] The much higher sensitivity of the mDSC (AC method) over DSC (DC method) permits use of much lower scan rates (1°C/min vs 10°C/min), and allows one to examine narrow thermal events, such as T_gs in aged selenides.[27] We find that the $\Delta H_{nr}(x)$ term (Fig. 5c, curve F) abruptly decreases by an order of magnitude to almost vanish (~0) as x increases to 19.5%, and to remain minuscule till x > 26.0% when

the term increases abruptly by an order of magnitude again to display a square-well like behavior. The global minimum in $\Delta H_{nr}(x)$ term in the 20% < x < 26% range, is the reversibility window, a feature characteristic of isostatic networks.[16]

We also examined the effect of aging samples at room temperature and separately at 240°C. In these measurements, glass samples in hermetically sealed Al pans were rerun 2 weeks after aging at room temperature, and these data (A1) appear in Fig. 5c as the open circles (red). All compositions except those in the 20% < x < 26%, show a general increase in the $\Delta H_{nr}(x)$ term upon aging with the step near x = 19.5% becoming abrupt but not the one near 26%. Samples at higher x (>26%) possess a T_g that exceeds 260°C.
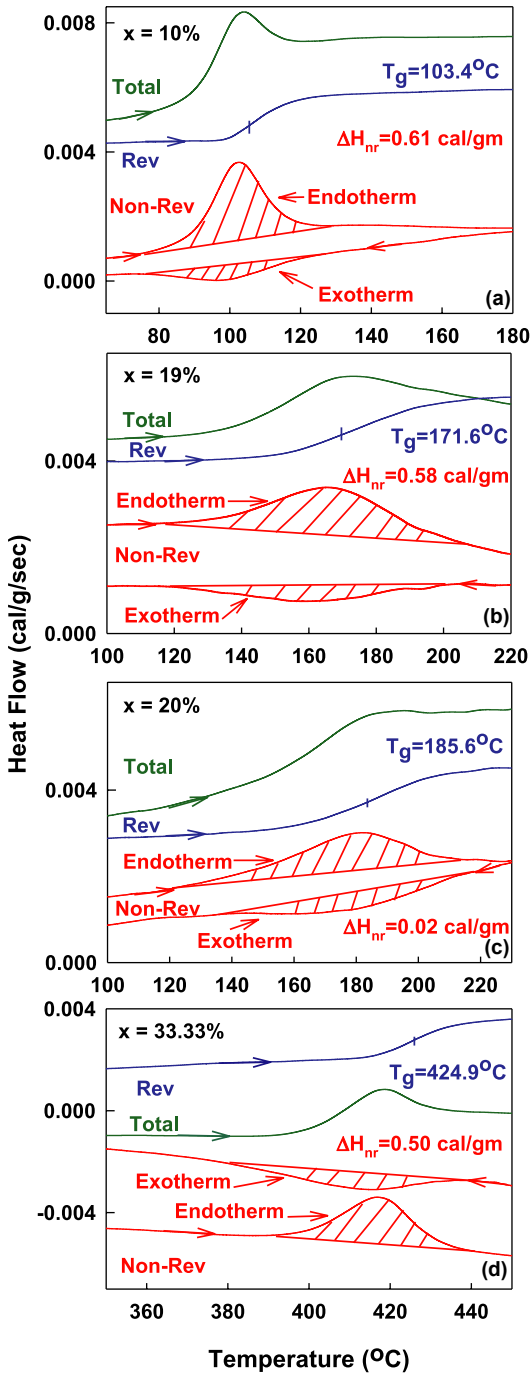
Fig. 4.   *Modulated – DSC scans of bulk Ge_xSe_{100-x} glasses at indicated glass compositions "x". Each panel shows four signals; the total, reversing and non-reversing heat flow in the heating cycle, and the non-reversing heat flow in the cooling cycle. Note that the enthalpy of relaxation, ΔH_{nr} term at x = 20% shows a global minimum, a composition in the IP.*
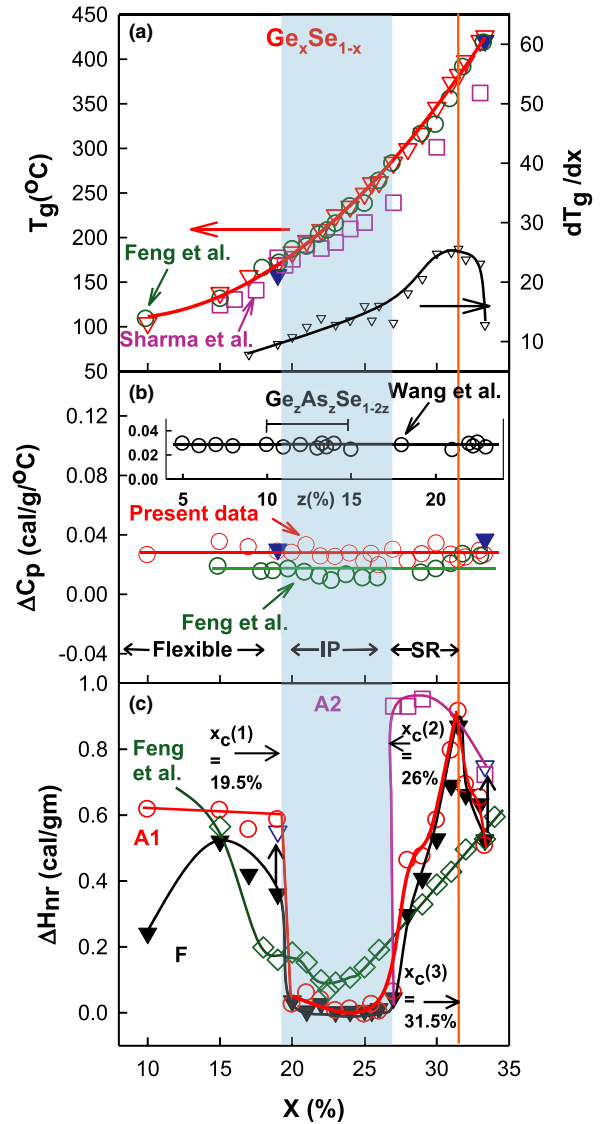

Fig. 5.   *Summary of mDSC results on Ge_xSe_{100-x} bulk glasses showing (a) variations in $T_g(x)$ ($\triangledown$) and dT_g/dx ($\triangledown$). (b) $\Delta C_p(x)$ and (c) non-reversing heat flow $\Delta H_{nr}(x)$. In panel (a) $T_g(x)$ from the work of Feng et al.[5] ($\bigcirc$), Sharma et al.[28] ($\square$) are included for comparison. T_g of wet samples ($\blacktriangledown$) at x = 19% and at x = 33.33% are included. In panel (b) $\Delta C_p(x)$ trends from Feng et al.[5] ($\bigcirc$) on Ge_xSe_{100-x} binary and Wang et al.[22] on the $Ge_xAs_xSe_{100-2x}$ ternary ($\circ$) are included. In panel (c), $\Delta H_{nr}(x)$ trends in fresh (F) glasses ($\blacktriangledown$), glasses aged (A1) for 2 weeks at RT ($\bigcirc$), glasses aged (A2) at 240º C for 2 weeks ($\square$) are included. Trends in $\Delta H_{nr}(x)$ reported by Feng et al. ($\diamondsuit$), displaying a near triangular variation with x is included for comparison. The increase in ΔH_{nr} term in wet ($\triangledown$) glasses is compared to that in dry ones ($\blacktriangledown$) at the arrows. See text.*
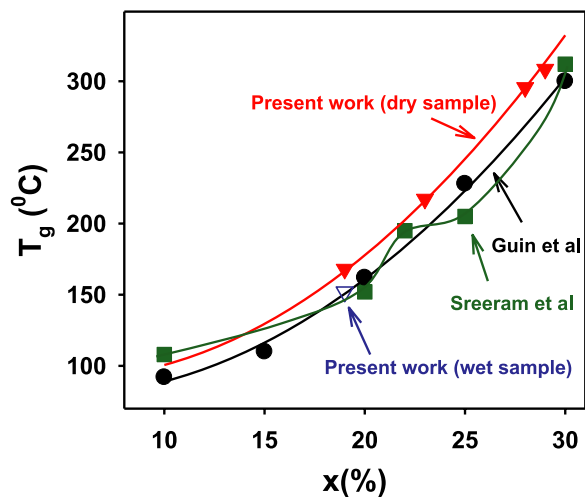
Fig. 6. Variation in DSC measured $T_g(x)$ in present dry (▼) and wet (▽) glasses compared with those reported earlier by Guin et al[25] (●), Sreeram et al[24] (■). The DSC scan rate in all measurements was kept at 10° C/min.

These glasses were aged at 240°C for 2 weeks, and the data (A2) reveal the $\Delta H_{nr}(x)$ term to now abruptly increase near $x = 26\%$. Several glass compositions, such as at $x = 30\%$, 31.5%, 32%, showed a small fraction of the glasses to crystallize upon aging at 240°C but not the ones at 27%, 28%, 29%, and 33.3%. XRD investigations show that the crystalline phase to nucleate is the metastable Ge_4Se_9 phase.[18]

Thermal properties of wet glasses differ from their dry counterparts as follows. T_gs of wet samples (Fig. 6) are lower than dry ones. Furthermore, $\Delta H_{nr}(x)$ in wet samples are measurably larger than in dry ones. These data form part of a systematic trend (Part I) that can be reconciled with bonded water producing dangling (Ge-OH and H-Se) ends.[28]

Molar Volumes and Network Packing

The *second* property of glasses of interest are their molar volumes, which show a broad minimum in the 20% < x < 26% range, the *reversibility window*, followed by a precipitous increase outside that window. We have also projected in the plot of Fig. 7, the $V_m(x)$ data for the two wet samples synthesized at $x = 19\%$ and 33.33%, and find that their $V_m(x)$ is lower than their dry counterparts, a behavior noted earlier in oxides[29] as well. At $x = 33.33\%$, the $V_m(x)$ reduction is

about 2.6%. At $x = 19\%$, close to the reversibility window, the reduction in $V_m(x)$ is much smaller, about 0.3%. We are aware of three previous studies[26,30,31] where rather complete $V_m(x)$ trends on the present binary are reported, and these data are included in the plot of Fig. 7. Our $V_m(x)$ trends are similar to previous reports but there are notable differences as well. In two cases[26,30] a broad minimum in $V_m(x)$ is also observed in the reversibility window but the increase of $V_m(x)$ outside the window is nearly halved, a feature that is probably due to glass heterogeneity. The $V_m(x)$ data of Feltz *et al.*[26] are about 2% lower than the Mahadevan data[30] across the board. These $V_m(x)$ (Fig. 7) results unequivocally show that glass compositions in the reversibility window form space filling networks.

Short range covalent forces determine the nature of local structures while long range ones determine network packing manifested in space filling. The global minimum in $V_m(x)$ in the IP is most likely the consequence of a minimal count of both floppy modes[12] and redundant bonds[12] in that phase, which permits the network as a whole to adapt and reconnect, expel stress and compact globally. The stress-free character of glass compositions in the IP was elucidated earlier in Pressure Raman experiments.[32] A critical externally applied pressure $P_c(x)$ could be identified when Raman modes first blue shift. The pressure $P_c(x)$ provides a measure of network stress, and displays a trend that closely mimics that of $\Delta H_{nr}(x)$. These data all strongly point to a new functionality of adaptation[6,7] acquired by networks in the narrow IP window that is ascribed to self-organization.

Optical Analog of the Reversibility Window

The *third* signature that batch compositions in the 19.5% < x < 26% window behave differently from those outside that window come from Raman lineshapes of the *as quenched melts* when compared to their T_g-*cycled glass* counterparts (Fig. 3). The Raman vibrational density of states (VDOS) of *as-quenched melts* at $x = 22\%$, and 24% appear remarkably similar to their T_g-*cycled glassy* counterparts. Raman VDOS at compositions both below ($x = 15\%$ and 17%) and above ($x = 31\%$ and 33%) that window show steadily increasing differences as one goes away from that window. Cooling melt compositions across T_g showing little or no change in molecular structure in the window
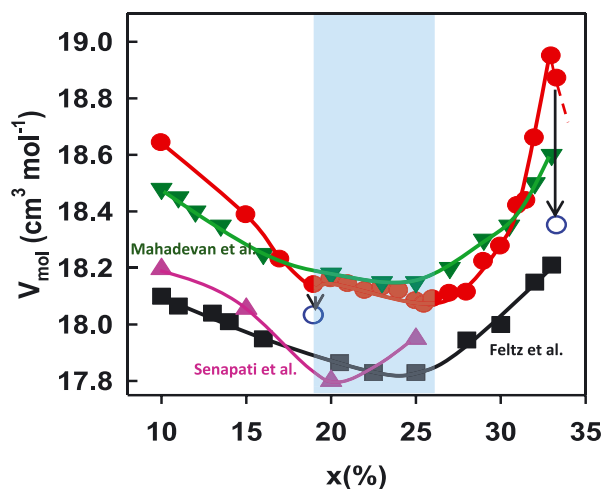
Fig. 7. Variations in molar volumes ($V_m(x)$) of present dry (●) and wet (○) Ge_xSe_{100-x} glasses are compared to earlier reports by Mahadevan et al.[30] (▼), Feltz et al.[26] (■), and Senapati et al[31] (▲). Note the much larger increase in $V_M(x)$ is observed at $x < 20\%$ and at $x > 26\%$ in the present set of samples than in earlier reports.

is a feature that is identified with *strong* melts. Melt compositions outside the window, such as at $x > 26\%$ (Fig. 3), not only show increased residual scattering and but also systematically higher concentration of edge-sharing (ES) units over CS ones compared to their T_g-cycled glass counterparts. Cooling such glass compositions across T_g leads to more ordered structures. In particular, at $x = 17\%$ and 15%, the scattering strength of the CS mode decreases substantially in the T_g-cycled glasses. Melts of batch compositions outside the IP clearly undergo substantial configurational changes upon structural arrest at T_g, and are viewed as fragile,[33] and possess an increased activation energy of viscosity as one goes away from the window.[16,34]

Raman Mode Scattering Strengths and Non-Stochastic Evolution of Glass Structure

Dispersive Raman measurements, performed at a fixed laser-power density at all glass compositions, have permitted establishing compositional variation of mode scattering strengths. In Figs. 8a–d, we plot the scattering strength variation of the CS ($I_{CS}(x)$) and ES ($I_{ES}(x)$) modes, and scattering strength ratios of chain-mode (CM) to CS mode ($I_{CM}(x)/I_{CS}(x)$), and separately ES to CS mode ($I_{ES}(x)/I_{CS}(x)$). We find $I_{CS}(x)$

varies linearly with x in the $0 < x < 33.3\%$ except for the $15\% < x < 26\%$ range. The linear variation is the expected *stochastic variation* as Ge atoms cross-link Se_n-chains of the base glass leading to a fully polymerized glass at $x = 33.33\%$. The *non-stochastic $I_{CS}(x)$ variation* in the $15\% < x < 26\%$ range, is also reflected in the $I_{CM}(x)/I_{CS}(x)$ variation; the Se_n-chain fragments decrease and the $GeSe_4$ CS-tetrahedra increase at a rate faster than the average behavior in the $15\% < x < 20\%$ range, but that behavior saturates in the $20\% < x < 26\%$ range (Figs. 8a and c), the IP. The faster growth rate clearly relates to onset of network rigidity as x approaches near 20%, while the saturation reflects the network adapting to expel stress in IP.[35]

Equally fascinating is the rich variation of $I_{ES}(x)$ (Fig. 8b); a slow increase in the $0\% < x < 19\%$ range, that slows down further in the $19\% < x < 26\%$, the IP, before increasing super-linearly in the $26\% < x < 31.5\%$ range with a power $n_1 = 2.30$, and super-linearly again in the nanoscale phase separated range, $31.5\% < x < 33.33\%$, but with a reduced power-law $n_2 = 1.40$. It is instructive to compare $I_{ES}(x)$ data with those of $I_{ES}(x)/I_{CS}(x)$. Both sets of data show a rapid conversion of CS units to ES ones at $x > 26\%$ (Figs. 8b and d) in the stressed-rigid regime. The rapid increase of the scattering strength ratio $I_{ES}(x)/I_{CS}(x)$ from 0.20 at $x = 26\%$ to 0.37 near $x = 33.33\%$ provides a convenient meeting point for many types of investigations on the present binary. To convert the Raman scattering strength ratio, $I_{ES}(x)/I_{CS}(x)$, into an ES/CS fraction, knowledge of the matrix element contributions is necessary. These were estimated[36] using cluster calculations, and the Raman cross-sections to excite the ES and CS modes were found, respectively, to be 40.5 and 47.9 A^4/amu. If one assumes a 10% error on these estimates, then the CS and ES Raman cross-sections become nearly the same, and the Raman $I_{ES}(x)/I_{CS}(x)$ ratios provide a good measure of the ES/CS fractions in the glasses. That view is independently corroborated from neutron structure factors, which place the ES/CS fraction at $x = 20\%$[37] and at $x = 33.33\%$[38] to be near 0.22(3) and 0.35(4), respectively. Recent ^{77}Se NMR experiments[39] also suggest that fraction to increase with x in harmony with the Raman and neutron scattering results (Fig. 8d). First-Principles calculation of the ^{77}Se NMR chemical shifts in $GeSe_4$ and $GeSe_2$ provide guidance on precise assignments of the NMR signals to specific local structures.[40] These theory results also rule out a simplistic inhomogeneous mixing of Se and $GeSe_2$ nanophases as a
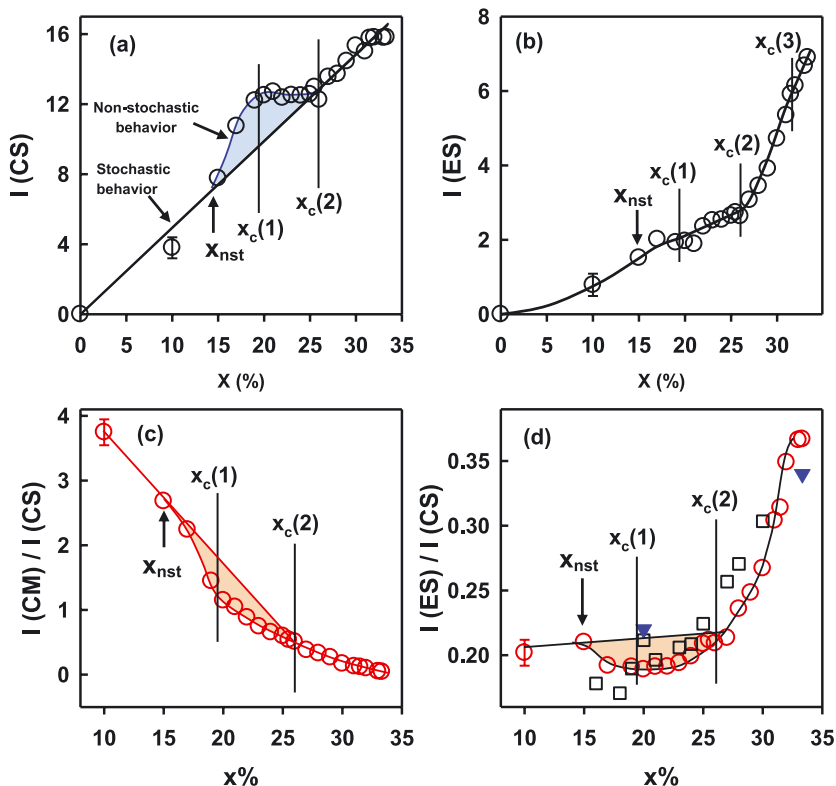
Fig. 8. Variation of Raman mode scattering strength of (a) CS mode ($I_{CS}(x)$) (b) ES mode ($I_{ES}(x)$), (c) and mode scattering strength ratio of CM to CS,($I(CM)/I(CS)$) and (d) of ES to CS, $I(ES)/I(CS)$ in the present binary. In (d), ($\square$) give ^{77}Se NMR results from ref. 39. ($\blacktriangledown$) give neutron scattering results from ref. 37 and 38. The linear variation of $I_{CS}(x)$ with x in (a) is the expected stochastic behavior. The departure from linearity shown by the shaded range, $15\% < x < 26\%$, is of non-stochastic origin. Trend in $I_{ES}(x)$ in (b) is almost linear in the $10\% < x < 26\%$ range, but power-law like at higher x. The markers $x_{nst}(x)$, $x_c(1)$, $x_c(2)$ and $x_c(3)$ represent, respectively, transitions in the onset of non-stochastic behavior, rigidity, stress, and nanoscale phase separation. See text for details.

possible description of these binary glasses (see ref. 17 in part I). We identify the rapid conversion of CS units to ES ones at $x > 26\%$ (Fig. 8d) to growth of the quasi 2D structural motifs based on the structure of α-GeSe$_2$ particularly as x exceeds 31.5% and glasses segregate into Ge-rich and Se-rich nanophases (see below). The structural motif also known as the outrigger raft is characterized by an ES/CS fraction of 0.50. Note that the ES/CS fraction in glasses rapidly increases with x to approach a value of 0.38 at x = 33.3% (Fig. 8) but never attains the value of 0.50 characteristic of the α-GeSe$_2$ structure.

The Three Elastic Phases

To further understand implications of the present results it is useful to compare predictions of

Rigidity theory with the present experimental data. The rigidity and stress transitions in amorphous networks are percolative in nature as shown by the Pebble game.[2] These simulations show isostatically rigid clusters first percolate at the Rigidity transition. With a further increase of network connectivity, redundant bonds first onset near the stress transition in the network at the second transition. In between these two elastic phase transitions, we have disordered networks that are rigid but stress-free. Numerical experiments place elasticity in the stressed-rigid phase to increase as a power-law in $\bar{r}$.[41,42] The power-law prediction was first confirmed in Raman optical elasticity and IR reflectance experiments.[43] The present Raman results on homogeneous glasses provide more accurate values of the underlying elastic power-laws.

Optical Elastic Power-Laws

The Stressed-Rigid Phase

CS- and ES- units form part of the network backbone in the present binary glasses. Their mode frequency squared provides a measure of network optical elasticity. Variations in the CS- and ES-mode frequency squared, $v^2(x)$ can be analyzed to extract optical elastic power-laws in the stressed-rigid (Figs. 9 and 10a and b) phase using the relation[41,42]

$$v^2 - v_c^2 = A(x - x_c)^p \qquad (2)$$

In eq. (2), v_c represents the Raman mode frequency at the elastic threshold composition x_c. Two methods were used to independently ascertain the power-law "p"; a polynomial fit using eq. (2), and separately a log-log plot to the $v(x)$ data as discussed elsewhere.[18] The dual approach works rather well, and the results (Figs. 10a and b) place the rigidity transition, $x_c(1) = 19.5\%$, the stress-transition $x_c(2) = 26.0(3)\%$, the optical elasticity power-law for CS mode, $p_2^{CS} = 1.50(3)$ and for ES mode, $p_2^{ES} = 1.47$ (3).

These power-laws (p_2^{CS} and p_2^{ES}) for the stressed-rigid phase from the CS and ES mode frequency variation give essentially the same value. This is as one would expect given that both local structural units form part of the same stressed-rigid backbone. These results are in harmony with the numerically predicted value of 1.50^{41} and 1.40^{42} using the standard random network model of glasses. These Raman results unequivocally show glassy networks formed at $x > x_c(2)$ in the present binary glasses are in the stressed-rigid phase.

The Intermediate Phase

We have also deduced the elastic power-law in the IP (Fig. 10c) using the variation of CS-mode frequency and find, $p_1 = 1.1(1)$. The analysis also yields a threshold value for the rigidity transition near $x_c(1) = 19.5$ (3)%. There are currently no theoretical predictions available for the elastic power-law in the IP, although this is not because of a lack of an attempt.[44]

In the present homogeneous samples, the abrupt variation in $\Delta H_{nr}(x)$ near the rigidity and stress transitions reflects the percolative nature of the two
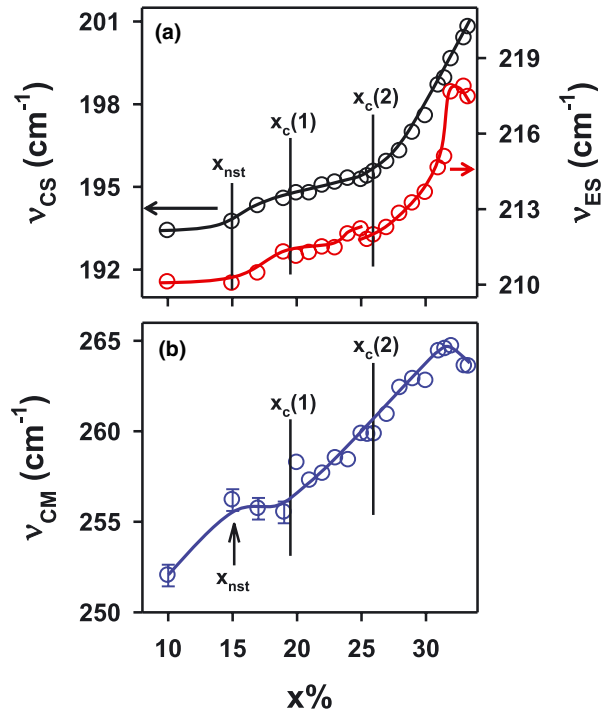

Fig. 9.   Compositional variation of (a) CS-, ES- mode frequency, $v_{CS}(x)$, $v_{ES}(x)$ (b) CM mode frequency $v_{CM}(x)$. The markers x_{nst}, $x_c(1)$, $x_c(2)$ are the same as in Fig. 8. See text.

elastic phase transitions.[2] The vanishing of the $\Delta H_{nr}(x)$ term in the IP reflects the intrinsically isostatic[16] nature of that phase. From a general viewpoint, such a result can be understood qualitatively from energy landscape approaches. At low connectivity (in the flexible Se-rich compositions), the energy of the system is dominated by the presence a few principal minima corresponding to the bond energy between Se atoms and between Ge and Se. The number of these minima is obviously proportional to $\bar{r}$, and contains also a contribution arising from floppy modes, because for each deformation mode, there are a certain number of associated energy minima. Overall, the complexity (the number of local minima) of the energy landscape is proportional to $\bar{r}$ which decreases when the concentration of Ge increases. At the other end, one has a rough energy landscape with an increased number of principal minima proportional to $\bar{r}$. In between, there is a compositional region where $\bar{r}$ is optimal and the fraction of floppy modes small, leading to a simple energy landscape where relaxation is optimized.
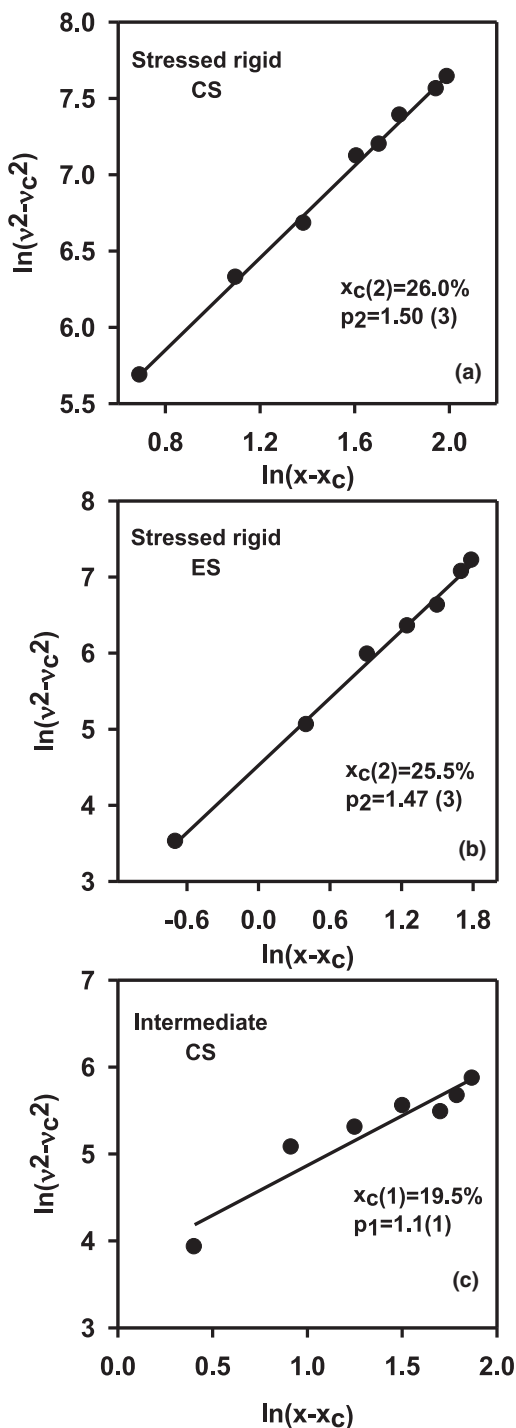
Fig. 10.   Elastic power-law (p) and threshold (x_c) deduced from (a) CS- (b) ES- mode frequency variation in the stressed-rigid phase, and (c) CS mode in the Intermediate phase. See text.

If one follows the models proposed for the IP[12,45] one finds changes at the thresholds defining the IP to be controlled by specific structural parameters. In the SICA approach,[45] the jump at the stress transition is controlled by the fraction of ES units, with a smaller jump when the ES fraction is increased. The structural signature of the stress transition as revealed in MD simulations[46,47] consists of asymmetric bending motion of angular excursions around the Ge atom when a network becomes stressed-rigid. The rigidity transition appears mostly controlled by energy considerations (loss of floppy modes) while the stress transition is driven by entropic considerations (large configurational changes). These effects are enhanced in multicomponent systems with several isostatic structures that also widen the IP width.[48] The present findings suggest that the sharpness of the reversibility window upon aging results from a conversion of ES tetrahedra to CS ones. Figure 3 shows that the intensity of the 217/cm mode corresponding to ES tetrahedra to decrease when a glass is T_g-cycled, i.e., relaxed (Fig. 3). These findings suggest that a decrease in the fraction of ES units upon aging correlates with the sharpness of the IP boundaries.

Sharpening of the Intermediate Phase Boundaries and Glass Homogeneity

The reversibility window in Ge_xSe_{100-x} glasses was examined in two previous reports. The data of Fig. 11a are taken from the first report on the subject by X.Feng et al.[5] in 1997, and the one in Fig. 11b from the second report[49] in 2009. In ref. 5, melts were reacted at 950°C for 2 days, while in ref. 49 they were reacted at 950°C for 4 days. The reversibility window from the present work (Fig. 11c) comes from melts that were reacted at 950°C for 7 days. It is useful to mention that the source of starting materials, their purity and lump size, batch size (2 g), and vacuum sealing was kept the same in all three set of investigations. The only variable was the reaction time, t_R of the starting materials at 950°C. These data of Fig. 11 highlight rather directly the crucial role of batch homogeneity on the sharpness of reversibility window.

The square-well like variation of $\Delta H_{nr}(x)$ in the present glasses of proven homogeneity (Fig. 11c), suggests a simple model for correlating the average window width $<W>$, and the width at $\Delta H_{nr}(x) = 0$, W_0, with the glass sample heterogeneity, Δx, characterizing fluc-

tuations of Ge-stoichiometry across a batch composition. We define <W> as the width between the midpoints of the walls of the reversibility window. As shown earlier in Part I, Raman profiling experiments permit measuring Δx directly. If we take $\Delta H_{nr}(x)$ to have a bimodal distribution, i.e., $\Delta H_{nr}(x) = 0$ in the reversibility window, and to take on a value of 1 cal/g outside the window (Fig. 12d), we can model the expected variation of $\Delta H_{nr}(x)$ as a function of the heterogeneity parameter Δx. Let us take <W> = W$_0$ = 6.5% at $\Delta x = 0$. Now, if the heterogeneity $\Delta x = 3\%$, then in its simplest form one can expect $\Delta H_{nr}(x)$ to vanish only near the window center, i.e., $x = 23\%$, and to display a triangular variation (Fig. 12a), a behavior reminiscent of the results (Fig. 11a) of X Feng *et al.*[4] Modeling results also show that the window width W$_0$ steadily increases as Δx decreases from 3% to 0%. The modeling results also place the average window width <W> to remain almost the same for heterogeneity variation in the 3% > $\Delta x > 0\%$ range (Fig. 13). At $\Delta x > 4\%$, the window depth begins to decrease, and at still higher Δx the window disappears. In glasses studied[49] in 2009, the observed reversibility window (Fig. 11b) width W$_0$ was found to be 4%, and the plot of Fig. 13 predicts the heterogeneity $\Delta x = 1\%$, in reasonable agreement to the Raman profiling results for the x = 19% glass sample reacted for $t_R = 96h$. The heterogeneity Δx is deduced from the spread in scattering strength ratio of the CS/ES vibrational modes in the observed lineshapes. Thus, the model introduced here provides a quantitative means to directly correlate calorimetric results on W$_0$ with glass heterogeneity, Δx, from Raman profiling experiments. An interesting spinoff of the model is that even when samples are not completely homogeneous, i.e., Δx is finite and less than 3%, one can reliably infer the <W> of the reversibility window by taking the separation between the midpoints of the walls (Fig. 13).

Our $T_g(x)$ results also reveal that for glass samples that possess a small heterogeneity, such as $\Delta x = 2.5\%$, the $T_g(x)$ variation is almost the same as found in the very homogeneous samples ($\Delta x = 0$). In Fig. 5a, note that the $T_g(x)$ variation of present homogeneous samples (smooth red line in Fig. 5a) nearly coincides with the $T_g(x)$ variation reported by Feng *et al.*[7] shown as green open circles. This is the case because $T_g(x)$ variation is a slowly varying function of x, and for heterogeneous samples, in effect, one averages T_g over two or
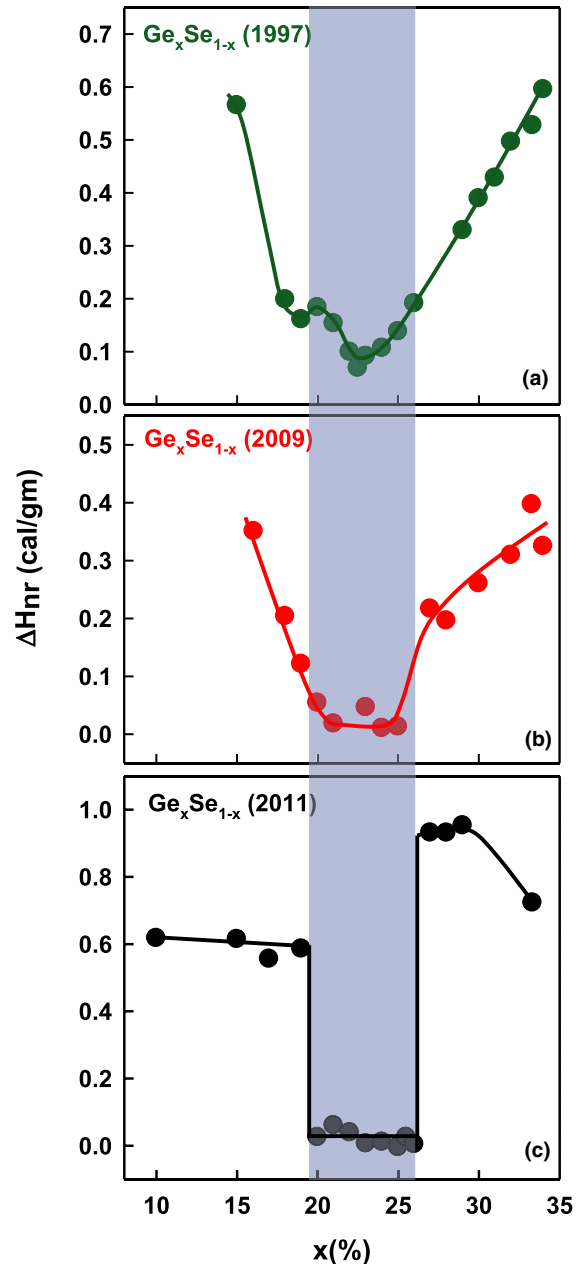

Fig. 11. Reversibility window in Ge$_x$Se$_{100-x}$ glasses reported (a) by Feng et al.[5] (1997), (b) Boolchand et al[49] (2009) and (c) Bhosle et al.[17] (2011). As glass samples homogenize (a→b→c) the reversibility window becomes square-well like.

three adjacent compositions. Thus, presence of some heterogeneity of glass composition is not reflected in T_g trends, but becomes transparent dramatically in the enthalpy of relaxation at T_g.

Fig. 13. Model prediction of reversibility window average width $<W>$ and the width W_o as a function of increasing glass heterogeneity (Δx).

Se-H dangling ends in the network are also responsible for the increase of the $\Delta H_{nr}(x)$ term as the glass softens near T_g. The heat intake upon glass softening due to these dangling ends is non-ergodic in nature, and it contributes to an increased non-reversing enthalpy as expected. These data underscore the crucial role of melt dryness, purity, and homogeneity to establish the intrinsic physical behavior of these nanostructured systems.
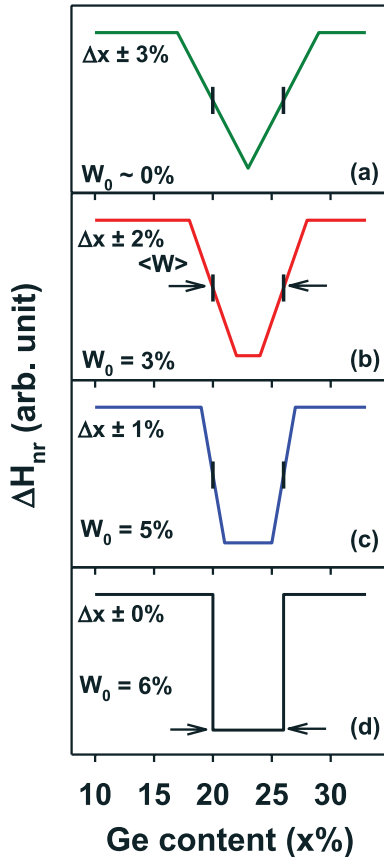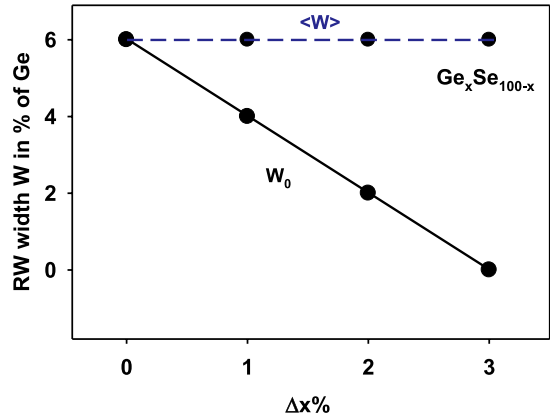
Fig. 12. Model variation of reversibility window from (d) a square-well like shape in homogeneous glasses (($\Delta x = 0$), (c) to a trapezoidal shape for glasses with some heterogeneity $\Delta x = 1\%$, and (b) $\Delta x = 2\%$, to (a) a triangular variation at $\Delta x = 3\%$. The average window-width, $<W>$, as measured by the spacing between the mid-point of the walls remains nearly constant in the $0\% < (\Delta x) < 3\%$ range. The part of the window corresponding to a vanishing $\Delta H_{nr}(x)$, i.e., W_o, steadily decreases as glass heterogeneity (Δx) increases.

The presence of water impurities in glasses, such as the one examined at $x = 19\%$ and 33.33% (Fig. 5a), leads to a rather large depression of T_g: from 171(1)°C to 158(1)°C at $x = 19\%$, and from 425 (1)°C to 420 (1)°C at $x = 33.33\%$. Furthermore, we observe a measurable increase in $\Delta H_{nr}(x)$ from 0.36(5) cal/g to 0.55 (5) cal/g at $x = 19\%$, and from 0.52(5) cal/g to 0.75 (5) cal/g at $x = 33.33\%$. These data are summarized in Table I of Paper I. The reduction in T_g is the natural consequence of bridging Se atom in the network (Ge-Se-Ge) being replaced by Ge-OH …H–Se–Ge. The same loss of connectivity that produces the Ge-OH and

Ideal Glasses, Melt Fragilities, and Intermediate Phases

The observation of a thermally reversing window correlates with Raman VDOS, which show little or no change across T_g (Fig. 3) for window compositions. This is a profound result, and raises fundamental issues. Both the calorimetric and optical data point to the fact that the configurational entropy change across T_g for these privileged IP compositions are minuscule, i.e., glassy networks in the IP possess liquid-like entropy. Not surprisingly, melt fragilities also reveal a minimum for IP compositions in the chalcogenides. Here the melt fragility data at $x > 25\%$ are difficult to obtain from traditional viscosity measurements because of the tendency of such melts to crystallize. Melts in the reversibility window not only display high glass-forming tendency,[1,50] but also form rigid and stress-free networks that hardly age. We associate these properties with self-organized glasses that are also ideal glasses in the sense that the glass-forming tendency is optimized.

The issue was discussed by J.C. Phillips a long time ago[50] when he identified regions of high glass-forming tendency with glass compositions that could be realized by slow cooling of melts. The results showed that the tendency is optimized for networks possessing a connectivity somewhat lower than the critical mean coordination number $\bar{r} = r_c = 2.40$, corresponding to the mean-field rigidity transition. An increase of cooling rate (from air quench to water quench) increased the glass-forming region up to $\bar{r} = 2.67$. Similarly, it has been recognized that[51,52] ideal glasses are those for which melt viscosity remains high even as temperature is lowered. For this reason, glasses form more easily at eutectics because of freezing-point depression, which brings the system to lower temperatures with high viscosity serving to inhibit crystallization. However, when comparing the phase diagram of the present binary with Fig. 5 (giving the IP), there is clearly no correlation between the location of an eutectic and the one of the IP. These findings show that it is, indeed, the flexibility and rigidity of networks that controls the ease of glass formation.

Our calorimetric results show $\Delta C_p(x)$ to be independent of x in the $10\% < x < 33.33\%$ range (Fig. 6b). We compare $\Delta C_p(x)$ data on the present samples with those reported by Feng *et al.*[5], and find that for both sets of data, within the errors of measurement, $\Delta C_p(x) = 0.035(5)$ cal/g/°C or 1.17R at $Ge_{20}Se_{80}$, where R represents the Gas constant of 8.3 Joule/mole/K. The C_p glass $(x = 20\%) = 0.06$ cal/g/°C below T_g, translates into a molar specific heat of 2.35R. The molar specific heat in the liquid C_p^{liquid} $(x = 20\%) = 3.51R$ at $T > T_g$, a value somewhat greater than the Dulong Petit value for $C_v = 3R$ in monotomic solids. This is as it should be given that $C_p = C_v + \alpha^2 TV/K_T$, where α and K_T represent, respectively, the thermal expansion and isothermal compressibility of the melt. A value of $\Delta C_p(x) = 0.035(5)$ cal/g/°C was also noted[22] earlier in ternary $Ge_xAs_xSe_{100-2x}$ glasses over a wide range of compositions x (Fig. 6b). These $\Delta C_p(x)$ data were obtained by analyzing the step in the reversing heat flow in mDSC experiments.

The mDSC results are compelling in suggesting that there appears little or no correlation between melt-fragilities and $\Delta C_p(x)$ in the present chalcogenides. The ΔC_p term remains independent of x over a wide composition range $(10\% < x < 33.3\%)$, a finding that is at odds with the view advanced by Angell.[53] On the other hand, melt fragilities (Fig. 14) correlate well with the enthalpy of relaxation $\Delta H_{nr}(x)$. The correlation appears physically appealing since both T_g and ΔH_{nr} are of non-ergodic origin, underscoring the non-equilibrium nature of the glass transition. The ΔC_p term is of ergodic origin and most likely of vibrational character, which should be distinguished from the ΔH_{nr} term that is largely configurational in nature.

The present work on chalcogenides glasses shows that ideal glasses rarely occur in monolithic stoichiometric systems like SiO_2, As_2S_3, B_2O_3 or $GeSe_2$. They form at non-stoichiometric compositions and particularly in multi-component systems[22,54,55] where numerous isostatic local structures can open wide compositional windows of self-organization. These new ideas are in contrast to the prevailing view of an ideal glass[53] realized by slow cooling stoichiometric melts to approach the configurational entropy close to that of the corresponding crystal at a low temperature, usually identified as the Kauzmann temperature.[56]

Onset of Nanoscale Phase Separation in Ge_xSe_{1-x} Glasses at $x > 31.5\%$

A chemically ordered continuous random network (COCRN) model description of the present glasses appeared in the early 1980s and gained popularity. Such a model requires that Ge-Ge bonds first appear once $x > 33.33\%$, the chemical threshold. The observation of
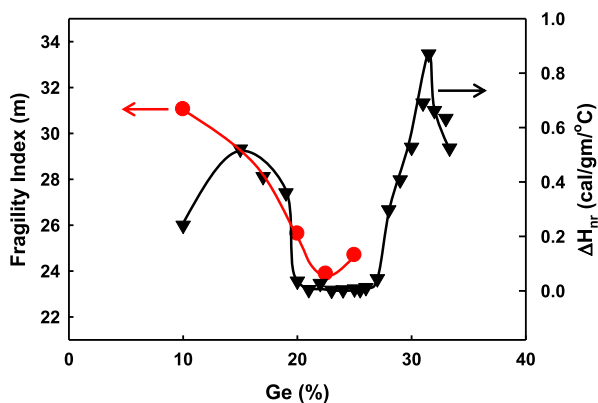

Fig. 14.   *Variations in melt fragility m(x) (●) from viscosity measurements by Stolen et al.[33] and in enthalpy of relaxation ΔH_{nr} term (▼) show a global minima in the Intermediate Phase.*

broken chemical order of $GeSe_2$ glass,[1,57,58] which initiates at $x > 31.5\%$ as Ge-Ge bonds first appear[23] in the network, is a feature of experimental data that are difficult to reconcile with a COCRN model. The maximum in the slope dT_g/dx near $x_c(3) = 31.5\%$ in the present glasses is the signature of segregation of Ge-Ge bonds in the network once they first nucleate. The structural evidence first emerged from [119]Sn Mossbauer spectroscopy[23] and Raman scattering[23] experiments. These Ge-Ge bonds form part of ethane-like units that apparently decouple or nanoscale phase separate from the backbone. The decoupling is suggested by the sudden decrease of the slope dT_g/dx, and the non-reversing enthalpy $\Delta H_{nr}(x)$ once $x > x_c(3)$ (Fig. 5c). Both T_g and ΔH_{nr} are network connectivity determined properties of glasses, and the lowering of the slope dT_g/dx and the ΔH_{nr} term at $x > x_c(3)$ reflects loss of network connectivity due to demixing of some of the excess Ge (at $x > x_c(3)$) from the backbone. In a COCRN model of these glasses, one expects stoichiometric glass at $x = 33.33\%$ to be chemically ordered.

As the Ge content of the glasses x exceeds 26%, the ES/CS fraction is found to increase (Fig. 8d), which provides evidence of a characteristic cluster based on the 2D form of $GeSe_2$ nucleating. This cluster was first introduced to account for chemical phase separation of the stoichiometric bulk $GeSe_2$ glass.[59] In α-$GeSe_2$, this cluster consists of pairs of ES tetrahedra that crosslink chains of CS ones, with an "ideal" ES/CS fraction of 0.5. The evidence that such a reconstructed cluster forms[60] at $x > 32\%$ in the glasses has come not only from the ES/CS fraction rapidly increasing towards that ideal value as x approaches 33.33% but also from the Raman vibrational signature of the Se–Se dimers that dress the edge of such a cluster. Late Professor Murase[60] showed that the mode near 246/cm in a $GeSe_2$ glass represents the Se–Se stretch of the dimers. A perusal of the Raman lineshapes of the present glasses (Fig. 1), shows that this particular mode, and a corresponding mode associated with Ge-Ge bonds to simultaneously grow in the 31% < x < 33.33% range as the network progressively demixes. These optical data confirm the nanoscale phase segregation of these glasses noted earlier in [129]I Mössbauer spectroscopy measurements,[57] which showed evidence of a finite concentration of I-Se bonds persisting all the way to $x = 33.33\%$. Independently, first-Principles MD simulations of liquid[61,62] and glassy $GeSe_2$ reveal pre-peaks in the pair distribution functions g_{GeGe} and g_{SeSe}, which are indicative of homopolar bonding. In summary, the present thermal measurements on T_g and $\Delta H_{nr}(x)$ along with earlier Raman and Mössbauer spectroscopy[23,57] results provide persuasive evidence for onset of nanoscale phase separation in the present binary once $x > x_c(3) = 31.5\%$.

Conclusions

Thermal, optical, and mechanical properties of homogeneous Ge_xSe_{100-x} glasses reveal sharply defined rigidity transition near $x_c(1) = 19.5(5)\%$ and stress transition near $x_c(2) = 26.0(5)\%$, with optical elastic power-laws in the Intermediate Phase (IP: 19.5% < x < 26.0%) of $p_1 = 1.10(10)$, and in the stressed-rigid phase ($x > 26.0\%$) of $p_2^{CS} = 1.50(3)$. These experiments supported by theory show present glasses to be intrinsically nanostructured displaying several distinct regimes of variation; at low x (<15%), Ge randomly cross-links Se_n-chains in the elastically flexible phase. But starting near $x > 15\%$, a *non-stochastic* variation of glass structure is manifested that continues through the IP (20% < x < 26%). In the IP networks acquire new functionalities including dynamical reversibility and non-aging, physical properties that one associates with self-organization. At higher x (26% < x < 31%) networks continue to be fully polymerized and are elastically stressed-rigid. At still higher x (>31.5%) networks segregate into Ge-rich and Se-rich nanophases. Melts containing traces of water homogenize much quicker than their dry counterparts but their physical properties including T_g, ΔH_{nr}, V_m are found to be measurably different from their dry counterparts. Rigidity theory has proved to be an invaluable tool to understanding the complex structural behavior of chalcogenide glasses,[49] modified oxides,[49] and solid electrolyte glasses.[49]

The real and imaginary parts of the specific heat $C_p(\omega)$, as a function of modulation frequency ω, have been studied using m-DSC. Compositional variation of melt fragility close to T_g were examined in the specially prepared homogeneous melt/glass samples. Results[63] show melt-fragility, m(x) to display a global minimum near $x = 23\%$. The fragility window coincides with the reversibility window centroid in composition space x. The result illustrates that glass compositions in the reversibility window give rise to strong melts, while compositions outside the reversibility window to fragile melts.

Acknowledgments

References

1. J. C. Phillips, "Topology of Covalent non-Crystalline Solids I: Short-Range Order in Chalcogenide Alloys," *J. Non-Cryst. Solids*, 34 [2] 153–181 (1979).

2. D. J. Jacobs and M. F. Thorpe, "Generic Rigidity Percolation: The Pebble Game," *Phys. Rev. Lett.*, 75 [22] 4051–4054 (1995).

3. Several books including review chapters by individuals active in the field of Rigidity Theory and relevant experiments on network glasses have appeared, and some are listed below: (a) Rigidity and Boolchand Intermediate Phases in Nanomaterials, Ed. M. Micoulaut and M. Popescu, in Optoelectronic Materials and Devices (INOE, Bucharest, 2009), Vol. 6. (b) Phase Transitions and Self-Organization in Electronics and Molecular Networks, Ed. M. F. Thorpe and J. C. Phillips (Kluwer Academic/Plenum Publishers, Cambridge, UK, 2001).

4. D. Selvanathan, W. J. Bresser, P. Boolchand, and B. Goodman, "Thermally Reversing Window and Stiffness Transitions in Chalcogenide Glasses," *Solid State Commun.*, 111 [11] 619–624 (1999).

5. X. W. Feng, W. J. Bresser, and P. Boolchand, "Direct Evidence for Stiffness Threshold in Chalcogenide Glasses," *Phys. Rev. Lett.*, 78 [23] 4422–4425 (1997).

6. M. A. Brière, M. V. Chubynsky, and N. Mousseau, "Self-Organized Criticality in the Intermediate Phase of Rigidity Percolation," *Phys. Rev. E*, 75 [5] 056108–056116 (2007).

7. J. Barre, A. R. Bishop, T. Lookman, and A. Saxena, "Adaptability and "Intermediate Phase" in Randomly Connected Networks," *Phys. Rev. Lett.*, 94 [20] 208701–208704 (2005).

8. P. Boolchand, D. G. Georgiev, and B. Goodman, "Discovery of the Intermediate Phase in Chalcogenide Glasses," *J. Optoelec. Advan. Mat.*, 3 [3] 703–720 (2001).

9. B. J. Madhu, H. S. Jayanna, and S. Asokan, "Evidence of an Intermediate Phase in Ternary Ge$_7$Se$_{93-x}$Sb$_x$ Glasses," *Eur. Phy. J. B – Condensed Matt. Comp. Sys.*, 71 [1] 21–25 (2009).

10. J. C. Mauro, "Topological Constraint Theory of Glass," *Am. Ceram. Soc. Bull.*, 90 [4] 31–37 (2011).

11. P. Boolchand, X. Feng, and W. J. Bresser, "Rigidity Transitions in Binary Ge-Se Glasses and the Intermediate Phase," *J. Non-Cryst. Solids*, 293 348–356 (2001).

12. M. F. Thorpe, D. J. Jacobs, M. V. Chubynsky, and J. C. Phillips, "Self-Organization in Network Glasses," *J. Non-Cryst. Solids*, 266 859–866 (2000).

13. D. G. Georgiev, P. Boolchand, H. Eckert, M. Micoulaut, and K. Jackson, "The Self-Organized Phase of Bulk P$_x$Se$_{1-x}$ Glasses," *Europhys. Lett.*, 62 [1] 49–55 (2003).

14. P. Boolchand, M. Micoulaut, and P. Chen, "Nature of Glasses;" *Phase Change Materials, Science and Applications*, eds., S. Raoux and M. Wuttig. Springer, Heidelberg, 37–60, 2009.

15. P. Boolchand, D. G. Georgiev, and M. Micoulaut, "Nature of Glass Transition in Chalcogenides," *J. Optoelec. Advan. Mat.*, 4 [4] 823–836 (2002).

16. M. Micoulaut, "Linking Rigidity With Enthalpic Changes at the Glass Transition and the Fragility of Glass-Forming Liquids: Insight From a Simple Oscillator Model," *J. Phys.: Condens. Matt.*, 22 [285101] 1–7 (2010).

17. S. Bhosle, K. Gunasekera, P. Chen, P. Boolchand, M. Micoulaut, and C. Massabrio, "Meeting Experimental Challenges to Physics of Network Glasses: Assessing the Role of Sample Homogeneity," *Solid State Commun.*, 151 1851–1855 (2011).

18. S. Bhosle, "Direct Evidence for Abrupt Rigidity and Stress Transitions in Dry and Homogeneous Bulk Ge$_x$Se$_{100-x}$ Glasses," M.S. Thesis, University of Cincinnati, (unpublished) 2011.

19. P. W. Anderson, "Through the Glass Lightly," *Science*, 267 [5204] 1615–1616 (1995).

20. P. Chen, P. Boolchand, and D. Georgeiv, "Long Term Aging of Selenide Glasses: Evidence of sub-T$_g$ Endotherms and pre-T$_g$ Exotherms," *J. Phys.: Condens. Matt.*, 22 [6] 065104 (2010).

21. L. C. Thomas, *Modulated DSC Technology, "Chapter 5: Measurement of Glass Transitions and Enthalpic Recovery"*, eds., T.A. Instruments Inc., 43–50, 2007. Available at http://www.TAInstruments.com (accessed January 15, 2012).

22. Y. Wang, P. Boolchand, and M. Micoulaut, "Glass Structure, Rigidity Transitions and the Intermediate Phase in the Ge-As-Se Ternary," *Europhys. Lett.*, 52 [6] 633–639 (2000).

23. P. Boolchand, and W. J. Bresser, "The Structural Origin of Broken Chemical Order in GeSe$_2$," *Philosophical Magazine B*, 80 [10] 1757–1772 (2000).

24. A. N. Sreeram, A. K. Varshneya, and D. R. Swiler, "Molar Volume and Elastic Properties of Multicomponent Chalcogenide Glasses," *J. Non-Cryst. Solids*, 128 [3] 294–309 (1991).

25. J.-P. Guin, T. Rouxel, V. Keryvin, J.-C. Sangleboeuf, I. Serre, and J. Lucas, "Indentation Creep of Ge-Se Chalcogenide Glasses Below Tg: Elastic Recovery and non-Newtonian Flow," *J. Non-Cryst. Solids*, 298 [2–3] 260–269 (2002).

26. A. Feltz, H. Aust, and A. Blayer, "Glass-Formation and Properties of Chalcogenide Systems XXVI: Permittivity and the Structure of Glasses As$_x$Se$_{1-x}$ and Ge$_x$Se$_{1-x}$," *J. Non-Cryst. Solids*, 55 [2] 179–190 (1983).

27. P. Chen, C. Holbrook, P. Boolchand, D. G. Georgiev, K. A. Jackson, and M. Micoulaut, "Intermediate Phase, Network Demixing, Boson and Floppy Modes, and Compositional Trends in Glass Transition Temperatures of Binary As$_x$S$_{1-x}$ System," *Phys. Rev. B*, 78 224208 (2008).

28. D. Sharma, S. Sampath, N. P. Lalla, and A. M. Awasthi, "Mesoscopic Organization and Structural Phases in Network-Forming Ge$_x$Se$_{1-x}$ Glasses," *Phys. B*, 357 [3–4] 290–298 (2005).

29. D. I. Novita and P. Boolchand, "Synthesis and Structural Characterization of dry AgPO$_3$ Glass by Raman Scattering, Infrared Reflectance, and Modulated Differential Scanning Calorimetry," *Phys. Rev. B*, 76 184205–184212 (2007).

30. S. Mahadevan, A. Giridhar, and A. K. Singh, "Elastic Properties of Ge-Sb-Se Glasses," *J. Non-Cryst. Solids*, 57 [3] 423–430 (1983).

31. U. Senapati and A. K. Varshneya, "Configurational Arrangements in Chalcogenide Glasses: A new Perspective on Phillips' Constraint Theory," *J. Non-Cryst. Solids*, 185 [3] 289–296 (1995).

32. F. Wang, S. Mamedov, P. Boolchand, B. Goodman, and M. Chandrasekhar, "Pressure Raman Effects and Internal Stress in Network Glasses," *Phys. Rev. B*, 71 [17] 174201–174208 (2005).

33. S. Stolen, T. Grande, and H.-B. Johnsen, "Fragility Transition in GeSe$_2$-Se Liquids," *Phys. Chem. Chem. Phys.*, 4 [14] 3396–3399 (2002).

34. P. Boolchand, G. Lucovsky, J. C. Phillips, and M. F. Thorpe, "Self-Organization and the Physics of Glassy Networks," *Phil. Mag.*, 85 [32] 3823–3838 (2005).

35. G. Chen, F. Inam, and D. A. Drabold, "Structural Origin of the Intermediate Phase in Ge-Se Glasses," *Appl. Phys. Lett.*, 97 [13] 131901–131903 (2010).

36. K. Jackson, A. Briley, S. Grossman, D. V. Porezag, and M. R. Pederson, "Raman-Active Modes of a-GeSe$_2$ and a-GeS$_2$: A First-Principles Study," *Phys. Rev. B*, 60 [22] R14985–R14989 (1999).

37. C. Massobrio, M. Celino, P. S. Salmon, R. A. Martin, M. Micoulaut, and A. Pasquarello, "Atomic Structure of the two Intermediate Phase Glasses SiSe$_4$ and GeSe$_4$," *Phys. Rev. B*, 79 [17] 174201 (2009).

38. I. Petri, P. S. Salmon, and H. E. Fischer, "Defects in a Disordered World: The Structure of Glassy GeSe$_2$," *Phys. Rev. Lett.*, 84 [11] 2413–2416 (2000).

39. E. L. Gjersing, S. Sen, and B. G. Aitken, "Structure, Connectivity, and Configurational Entropy of Ge_xSe_{100-x} Glasses: Results From ^{77}Se MAS NMR Spectroscopy," *J. Phys. Chem. C*, 114 [18] 8601–8608 (2010).

40. M. Kibalchenko, J. R. Yates, C. Massobrio, and A. Pasquarello, "Structural Composition of First-Neighbor Shells in $GeSe_2$ and $GeSe_4$ Glasses From a First-Principles Analysis of NMR Chemical Shifts," *J. Phys. Chem. C*, 115 [15] 7755–7759 (2011).

41. H. He and M. F. Thorpe, "Elastic Properties of Glasses," *Phys. Rev. Lett.*, 54 [19] 2107–2110 (1985).

42. D. S. Franzblau and J. Tersoff, "Elastic Properties of a Network Model of Glasses," *Phys. Rev. Lett.*, 68 [14] 2172–2175 (1992).

43. P. Boolchand, M. Jin, D. I. Novita, and S. Chakravarty, "Raman Scattering as a Probe of Intermediate Phases in Glassy Networks," *J. Raman Spectrosc.*, 38 [6] 660–672 (2007).

44. M. Chubynsky, "Characterizing the Intermediate Phases Through Topological Analysis in the Intermediate Phase of Network Glasses;" *Rigidity Transitions and Boolchand Intermediate Phases in Nanomaterials*, eds., M. Micoulaut and M. Popescu. INOE, Bucharest, 213–261, 2009.

45. M. Micoulaut and J. C. Phillips, "Rings and Rigidity Transitions in Network Glasses," *Phys. Rev. B*, 67 [10] 104204–104209 (2003).

46. M. Bauchy, M. Micoulaut, M. Celino, S. Le Roux, M. Boero, and C. Massobrio, "Angular Rigidity in Tetrahedral Network Glasses With Changing Composition," *Phys. Rev. B*, 84 [5] 054201 (2011).

47. M. Micoulaut, C. Otjacques, J.-Y. Raty, and C. Bichara, "Understanding Phase-Change Materials From the Viewpoint of Maxwell Rigidity," *Phys. Rev. B*, 81 [174206] 1–11 (2010).

48. M. Micoulaut, "Rigidity and Intermediate Phases in Glasses Driven by Speciation," *Phys. Rev. B*, 74 [18] 184208–184205 (2006).

49. P. Boolchand, P. Chen, D. I. Novita, and B. Goodman, "New Perspectives on Intermediate Phases;" *Rigidity and Boolchand Intermediate Phases in Nanomaterials*, eds., M. Micoulaut and M. Popescu. INOE, Bucharest, 1–37, 2009.

50. R. Azoulay, H. Thibierge, and A. Brenac, "Devitrification Characteristics of Ge_xSe_{1-x} Glasses," *J. Non-Cryst. Solids*, 18 [1] 33–53 (1975).

51. F. Yonezawa, "Glass Transition and Relaxation of Disordered Structures;" *Solid State Physics*, eds., H. Ehrenreich and D. Turnbull. Academic Press, Boston, 179–238, C171–C178, 239–254, 1991.

52. P. Richet, "Viscosity and Configurational Entropy of Silicate Melts," *Geochim. Cosmochim. Acta*, 48 [3] 471–483 (1984).

53. C. A. Angell, "Glass Formation and the Nature of the Glass Transitions;" *Insulating and Semiconducting Glasses*, ed., P. Boolchand. World Scientific, Singapore; River Edge, NJ, 1–51, 2000.

54. T. Qu, D. G. Georgiev, P. Boolchand, and M. Micoulaut, "The Intermediate Phase in Ternary $Ge_xAs_xSe_{1-2x}$ Glasses;" *Supercooled Liquids, Glass Transition and Bulk Metallic Glasses*, eds., T. Egami, A. L. Greer, A. Inoue and S. Ranganathan. Materials Research Society, Pittsburgh, PA, 157, 2003.

55. S. Chakravarty, D. G. Georgiev, P. Boolchand, and M. Micoulaut, "Ageing, Fragility and the Reversibility Window in Bulk Alloy Glasses," *J. Phys.-Condensed Matt.*, 17 [1] L1–L7 (2005).

56. W. Kauzmann, "The Nature of the Glassy State and the Behavior of Liquids at Low Temperatures," *Chem. Rev.*, 43 [2] 219–256 (1948).

57. W. J. Bresser, P. Boolchand, and P. Suranyi, "Rigidity Percolation and Molecular Clustering in Network Glasses," *Phys. Rev. Lett.*, 56 [23] 2493–2496 (1986).

58. P. S. Salmon, A. C. Barnes, R. A. Martin, and G. J. Cuello, "Glass Fragility and Atomic Ordering on the Intermediate and Extended Range," *Phys. Rev. Lett.*, 96 [23] 235502–235504 (2006).

59. P. M. Bridenbaugh, G. P. Espinosa, J. E. Griffiths, J. C. Phillips, and J. P. Remeika, "Microscopic Origin of the Companion A_1 Raman Line in Glassy $Ge(S,Se)_2$," *Phys. Rev. B*, 20 [10] 4140–4144 (1979).

60. K. Murase, "Vibrational Exciatation in Glasses: Raman Scattering;" *Insulating and Semiconducting Glasses*, eds., P. Boolchand. World Scientific, Singapore; River Edge, NJ, 415–464, 2000.

61. M. Micoulaut, R. Vuilleumier, and C. Massobrio, "Improved Modeling of Liquid $GeSe_2$: Impact of the Exchange-Correlation Functional," *Phys. Rev. B*, 79 [21] 214205 (2009).

62. M. Micoulaut and C. Massobrio, "Improving the Structural Description of High-Temperature Liquid $GeSe_2$ From *ab Initio* Molecular Dynamics Simulations," *J. Optoelec. Advan. Mat.*, 11 [12] 1907–1914 (2009).

63. K. Gunasekera, P. Chen, P. Boolchand, and M. Micoulaut, "Fragility, Reversibility and Window of Self Organization in Chalcogenide Glasses," in preparation.